International Journal of Mechanical, Industrial and Aerospace Sciences
ISSN: 2517-9950
Vol:6, No:12, 2012

Molecular Dynamics Simulation of Lubricant Adsorption and Thermal Depletion Instability

Bei Li, Qiu B. Chen, and Chee H. Wong

***Abstract*—**In this work, we incorporated a quartic bond potential into a coarse-grained bead-spring model to study lubricant adsorption on a solid surface as well as depletion instability. The surface tension density and the number density profiles were examined to verify the solid-liquid and liquid-vapor interfaces during heat treatment. It was found that both the liquid-vapor interfacial thickness and the solid-vapor separation increase with the temperatureT^* when $T^*$is below the phase transition temperature T_c^*. At high temperatures ($T^*>T_c^*$), the solid-vapor separation decreases gradually as the temperature increases. In addition, we evaluated the lubricant weight and bond loss profiles at different temperatures. It was observed that the lubricant desorption is favored over decomposition and is the main cause of the lubricant failure at the head disk interface in our simulations.

***Keywords*—**Depletion instability, Lubricant film, Thermal adsorption, Molecular dynamics (MD).

I. Introduction

PERFLUOROPOLYETHERS (PFPEs) have been widely used as the lubricants to reduce friction and wear between flying heads and rotating disks for hard disk drives (HDDs). Because of the superior properties, such as low surface tension, good load carrying, and low friction coefficient, PFPE is dip-coated onto a diamond-like-carbon (DLC) overcoat to serve as the first line of defense in the event of slider-to-disk intermittent contacts. However, the demands of achieving ultrahigh areal data density for HDDs have raised critical technical limitations in the head disk interface (HDI).One of such limitations is the slider flying height that is approaching to atomic scale, i.e., the recording head is flying over the disk surface at a height of less than 8 nm[1]. Under such a low spacing, the lubricant adsorption on the disk surface becomes increasingly essential to maintain the performance and reliability of the HDI. In addition, the size of magnetic grains on the disk has to be reduced accordingly, which causes another limitation in the HDI. Unfortunately, the recording bit becomes thermally unstable when its size is scaled down below the superparamagnetic limit (of the order of 10 nm)[2]. Heat assisted magnetic recording (HAMR) is viewed as a promising method to address the thermal effect thereby increasing areal data density beyond 1Tbit/in^2[3, 4]. In HARM, high coercivity magnetic medium can be used with the aid of a laser beam, which temporarily heats the medium above its Curie temperature (around 700K), making it easier to be overwritten. Due to the high laser heating rate used in HAMR (of the order of 10^{11}-10^{12}K/s), the temperature increases in a few nanoseconds and induces severe lubricant desorption and decomposition challenges associated with the use of ultrathin PFPE lubricants [5-8]. As such, it is of fundamental importance to study the lubricant adsorption on the disk surface as well as the lubricant thermal depletion instability at the HDI for HAMR-based HDDs.

In this work, we use molecular dynamics (MD) simulation to study the thermal-induced desorption and decomposition of molecularly thin lubricants at various temperatures. The number density and the surface tension density will be calculated to verify the lubricant adsorption on the disk surface under heat treatment. Lastly, the lubricant weight and bond loss profiles will be examined to investigate the thermal stability and durability of PFPEs at the HDI.

B. Li, Q.B. Chen, and C.H. Wong are with the School of Mechanical and Aerospace Engineering, Nanyang Technological University, 50 Nanyang Avenue, Singapore 639798, Singapore (phone: +65 6790 5913; fax: +65 6792 4062; e-mail: chwong@ntu.edu.sg).

II. Numeric Model and Methodology

A coarse-grained bead-spring polymer model is utilized in our simulations to simplify the detailed atomic information, which also maintains the essence of the internal molecular structures[9]. Each polymeric molecule consists of N_p beads and the bead number is related to the MW of the polymer chain. In our work, we investigate the nonfunctional lubricant PFPE Z2000, which consists of 10 identical beads per chain, to carry out preliminary studies on the phenomena of thermal-induced desorption and decomposition. Our previous results [10] showed that wall roughness has a slight effect on the van der Waals interaction between the lubricant and the wall. As such, to save the computation time, the smooth disk surface that lies on the x-y plane is regarded as a thermally inert, infinitely long, and infinitely deep flat surface, and is located at $z = 0$.

A. Potential Energy Functions

The van der Waals interaction between all the beads is expressed by a truncated-shifted "12-6" form of Lennard-Jones potential and is given as:

$$U_{LJ}(r) = 4\varepsilon\left[\left(\frac{\sigma}{r}\right)^{12} - \left(\frac{\sigma}{r}\right)^{6} - \left(\frac{\sigma}{r_c}\right)^{12} + \left(\frac{\sigma}{r_c}\right)^{6}\right] \quad (1)$$

where σ refers to the bead diameter, ε is the potential depth for the interaction between the beads, and r is the bead distance. The cutoff r_c is chosen to be 3.0σ to save the computation time.

To account for the interactions between the beads and the solid disk (wall) surface, a "9-3" form of the Lennard-Jones potential is used and is described as:

$$U_w(z) = \varepsilon_w\left[\frac{2}{15}\left(\frac{\sigma}{z}\right)^{9} - \left(\frac{\sigma}{z}\right)^{3}\right] \quad (2)$$

where subscript w refers to the disk surface, ε_w denotes the potential depth for the interaction between the bead and the wall, and z is the distance between the bead and the wall.

A quartic bond potential [11, 12]is employed to describe intrinsic bond breakage for coarse-grained model, which also mimics the finitely extensible nonlinear elastic (FENE) potential at the potential minimum. This quartic bond potential is computed as:

$$U_4(r)=\begin{cases}k_4(y-b_1)(y-b_2)y^2+U_0 & r<r_b\\ U_0 & r>r_b\end{cases} \quad (3)$$

where r is the bond length, $y = r - r_b$ shifts the quartic center from the origin, and $r_b$is the cutoff length at which the potential goes smoothly to a local maximum. When the bond length exceeds r_b, the bond will break and the quartic term is turned off to prevent bond from reforming. The parameters are chosen to be $k_4 = 1434.3\varepsilon/\sigma^4$, $b_1 = -0.7589\sigma$, $b_2 = 0.0$, $r_b = 1.5\sigma$, and $U_0 = 67.2234\varepsilon$[11, 12]to fit the quartic bond potential with the FENE potential at the minimum.

B. Simulation Details

We select σ, ε, m and τ ($\tau=\sigma\sqrt{m/\varepsilon}$) as the fundamental quantities in the MD simulations, where m is the mass of the bead and τ is the time unit. The time step $\Delta\tau$ is chosen to be 0.005τ to improve the computation efficiency. The equilibrium bond length is maintained at around 0.97σ, which is the typical value for polymeric liquid [13]. Periodic boundary conditions are applied to the x and y directions of the simulation box, while keeping the$z$ direction in a fixed boundary condition with sufficient domain height to provide a free lubricant-vacuum interface.

In our work, we incorporate the Langevin thermostat into the simulations to study lubricant desorption and decomposition at various temperatures. The Langevin equation [13]governs the Brownian motion for the ith bead in the ath lubricant molecule, such that

$$m\frac{d^2\mathbf{r}_{ai}}{dt^2}=-\frac{\partial U}{\partial\mathbf{r}_{ai}}-\zeta\frac{d\mathbf{r}_{ai}}{dt}+\mathbf{f}_{ai}(t) \quad (4)$$

where U is the total potential exerted on the ith bead. ζ is the friction coefficient that couples the beads to a heat bath, i.e., $\zeta=\Gamma\mathbf{I}$, where $\Gamma=0.5\tau^{-1}$ and $\mathbf{I}$ is the unit dyad. $\mathbf{f}_{ai}(t)$ is the Brownian random force due to the motion of ambient molecules. This random force obeys the Gaussian white noise and follows the fluctuation-dissipation theorem [13]as:

$$\langle\mathbf{f}_{ai}(t)\mathbf{f}_{bj}(t')\rangle=2k_BT\Gamma\delta_{ab}\mathbf{I}\delta_{ij}\delta(t-t') \quad (5)$$

where δ_{ab} and δ_{ij} are Kronecker deltas and $\delta(t\text{-}t')$ is the Dirac's delta function. The angular bracket indicates an ensemble average for this random force.

Initially, the system is relaxed in a canonical ensemble (NVT) for 2500τ at a constant temperature of $T^*=k_BT/\varepsilon = 1.0$. Then, the lubricant is uniformly coupled to an external heat bath with a constant heating rate of $0.0005\varepsilon/(k_B\tau)$. When the system is heated up to a desired temperature, it will be kept constant for another period of 10000τ. The time averaged quantities of interest will then be recorded over the following next 1000τ.

III. Results and Discussion

A. Calculation of the Surface Tension

In our simulations, with the wall located at $z = 0$ and lubricant at $z> 0$, the surface tension of the lubricant can be described as

$$\gamma=\int_0^{L_z}dz\left[p_N(z)-p_T(z)-n(z)z\frac{\partial U_w(z)}{\partial z}\right] \quad (6)$$

where $p_N(z)$ and $p_T(z)$ are the normal and transverse components of the pressure sensor respectively, $n(z)$ is the number density and U_w is the wall potential as expressed in (2). L_x, L_y and L_z are the domain lengths in x, y and z directions, respectively. To calculate this integral, the simulation box is divided into N_s slabs equally in the z-direction perpendicular to the wall with a slab thickness of $L_z/N_s = 0.2\sigma$. These slabs are parallel to the x-y plane and according to the statistic mechanical expressions [14, 15], the normal and transverse components of the pressure tensor for the kth slab can be derived as:

$$p_N(k)=k_BT\langle n(k)\rangle-\frac{1}{2V_s}\left\langle\sum_{i\in\Omega_k}\sum_{j\in\Omega_{ki}}\frac{z_{ij}^2}{r_{ij}}\frac{\partial U(r_{ij})}{\partial r_{ij}}\right\rangle \quad (7)$$

$$p_T(k)=k_BT\langle n(k)\rangle-\frac{1}{2V_s}\left\langle\sum_{i\in\Omega_k}\sum_{j\in\Omega_{ki}}\frac{1/2(x_{ij}^2+y_{ij}^2)}{r_{ij}}\frac{\partial U(r_{ij})}{\partial r_{ij}}\right\rangle \quad (8)$$

where $V_s = L_xL_yL_z/Ns$ is the slab volume, $n(k)$ is the density $n(z)$ averaged in kth slab, and $U(r_{ij})$ is the total potential exerted on ith bead by surrounding jth bead. Here, Ω_k denotes the beads that are located in kth slab. Ω_{ki} denotes the neighboring beads for bead i (bead $i\subset\Omega_k$). Note that for every bead in Ω_k, only half of the pair potential contributes to the pressure tensor calculation. Therefore, if beads i and j are both in the kth slab, a full pair potential will be used to calculate the pressure tensor.

Substituting (7) and (8) into (6), we obtain

$$\gamma=\sum_{k=1}^{N_s}\gamma(k)\quad k=1,2,...,N_s \quad (9)$$

where

$$\gamma(k)=\frac{L_z}{N_s}\left[p_N(k)-p_T(k)\right]-\int_{(k-1)L_z/N_s}^{kL_z/N_s}\left[n(z)z\frac{\partial U_w(z)}{\partial z}\right]dz$$
$$=\frac{1}{2L_xL_y}\left\langle\sum_{i\in\Omega_k}\sum_{\substack{j\in\Omega_{kl}\\ i\neq j}}\frac{1/2\left(x_{ij}^2+y_{ij}^2\right)-z_{ij}^2}{r_{ij}}\frac{\partial U(r_{ij})}{\partial r_{ij}}\right\rangle \quad (10)$$
$$-\int_{(k-1)L_z/N_s}^{kL_z/N_s}\left[n(z)z\frac{\partial U_w(z)}{\partial z}\right]dz$$

As an example, Fig. 1 shows the surface tension density profile of the lubricant at T^* = 1.0 as averaged over 1000τ. In a bulk phase, the pressure tensor is the same in both the normal and transverse directions so the term $p_N(z) - p_T(z)$ vanishes. Meanwhile, the bulk phase is situated over from plane $z = 4\sigma$, which indicates that the wall potential $U_w(z)$ becomes negligible for bulk phase. Therefore, according to (6), the surface tensions of bulk liquid phase γ_l and bulk vapor phase γ_v, should approach to zero as observed in Fig. 1. The total surface tension can then be separated into individual interface surface tension, i.e., solid-liquid interface surface tension γ_{sl}, and liquid-vapor interface surface tension γ_{lv}. Furthermore, the strong oscillations inγ_{sl} are consistent with the vibrations in the density $\rho_{sl}(z)$ of the solid-liquid interface, while the bulge in γ_{lv} corresponds to the smooth decrease in the liquid-vapor interface's density $\rho_{lv}(z)$ (as shown in Fig. 2).

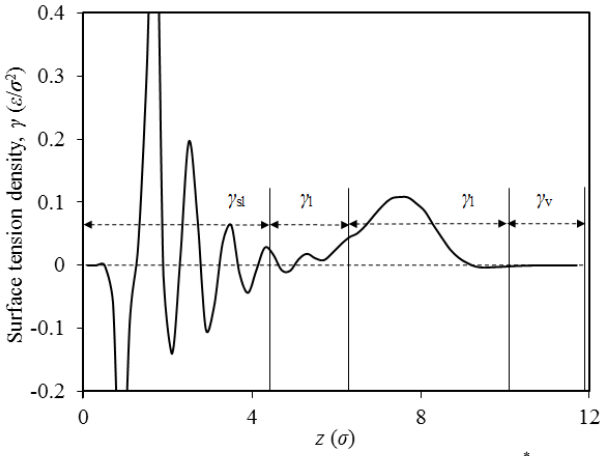

Fig. 1 Surface tension density profile of lubricant films at T^* = 1.0 as averaged over 1000τ

B. Determination of Liquid-Vapor and Solid-Vapor Interfacial Thickness

The liquid phase is very small in the surface tension density profile (Fig. 1), which makes it difficult to distinguish the solid-liquid and liquid-vapor interfaces clearly. To estimate the interfaces' locations accurately, both the surface tension density and number density profiles are taken into account.

Similarly, the number density profile can be obtained by dividing the simulation box into N_s slabs equally and counting the number of beads in each one. Fig. 2 depicts the density profile of the lubricant at T^* = 1.0with solid-liquid and liquid-vapor interfaces. Initially, the lubricant density oscillates

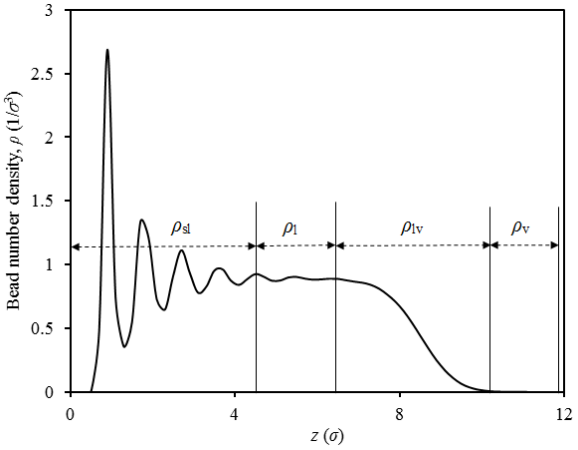

Fig. 2 Bead number density profile of lubricant films at T^* = 1.0 as averaged over 1000τ

strongly and reaches a maximum value near the base of the simulation box. This maximum peak is caused by the closely-packed lubricant molecules attached onto the wall in the first layer. Moreover, another three peaks are observed sequentially before a stable constant density ρ_l is achieved. This constant ρ_l indicates the bulk liquid phase in the density profile. Subsequently, the lubricant density $\rho(z)$ decreases smoothly from ρ_l to another stable constant density ρ_v, which represents the density of the vapor phase. Moreover, $\rho_{sl}(z)$ and $\rho_{lv}(z)$, as shown in Fig. 2, denote the solid-liquid interface's density and liquid-vapor interface's density, respectively. It is known that the liquid-vapor interface's density $\rho_{lv}(z)$ is usually described in the form of a hyperbolic tangent function, which is imposed by the van der Waals theory of surface tension [16-18] as:

$$\rho_{lv}(z)=\frac{1}{2}(\rho_l+\rho_v)-\frac{1}{2}(\rho_l-\rho_v)\tanh\left[\frac{2(z-z_0)}{\delta}\right] \quad (11)$$

with the liquid-vapor interfacial thickness δ defined by:

$$\delta=-\frac{\rho_l-\rho_v}{\left[\partial\rho_{lv}(z)/\partial z\right]_{z=z_0}} \quad (12)$$

This tangent function appears to be an odd function of z-origin z_0, which is given by $\rho_{lv}(z_0) = (\rho_l + \rho_v)/2$. Then we can calculate the solid-vapor separation $d = z_0 + \delta/2$ as the distance between the wall and the vapor phase. Therefore, only the lubricant molecules that lie above the plane $z = d$ contribute to the calculation of the lubricant weight loss profile in the following section.

In this work, the liquid-vapor interface's density $\rho_{lv}(z)$ is numerically interpreted by fitting the density profile with (11) over the range $z = 5\sigma$ to $z = 18\sigma$ as shown in Fig. 3. The density profile represents a steep liquid-vapor interface at low temperature and a broader interface as temperature increases. Once the temperature reaches a critical value, i.e., T_c^* = 2.2, the

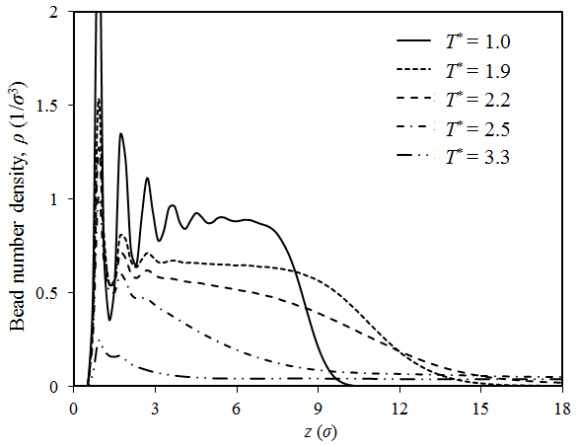

Fig. 3 Bead number density profiles of solid, liquid and vapor phases at coexistence for different temperatures as averaged over 1000τ

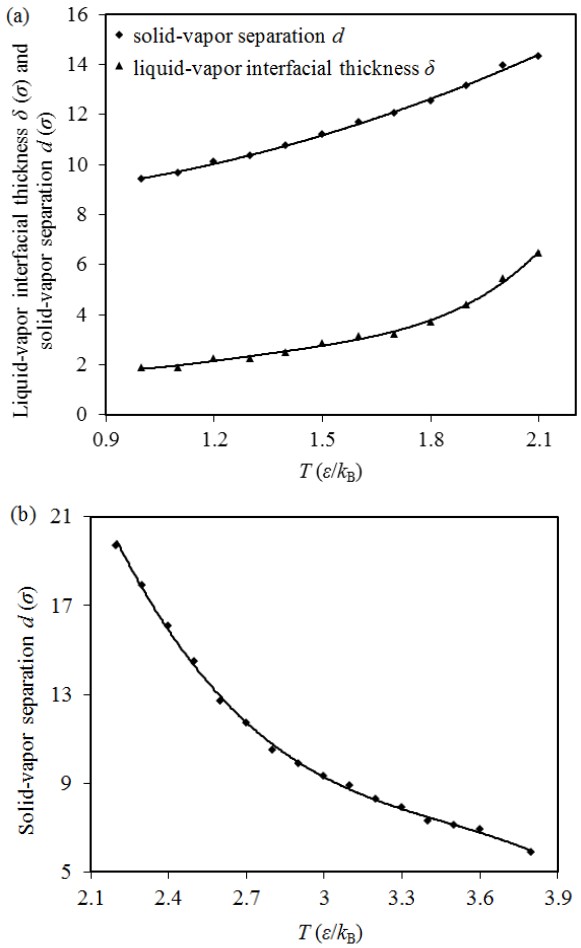

Fig. 4 (a) Liquid-vapor interfacial thickness δ and solid-vapor separation d when liquid phase exists; (b) solid-vapor separation d when liquid phase vanishes, for lubricant films at various temperatures

liquid phase would vanish and only one solid-vapor interface at $T^* = 2.5$ and $T^* = 3.3$ can be observed. As such, at $T^* \geq T_c^*$, we estimate the solid-vapor separation d as the distance, beyond which the density profile starts to approach to the constant vapor density ρ_v. Fig. 4 demonstrates the solid-vapor separation d for the lubricant at various temperatures. In Fig. 4(a), the liquid phase is bounded between the wall and the vapor phase. Both the liquid-vapor interfacial thickness δ and solid-vapor separation d increase monotonously with the temperature. However, at high temperatures ($T^* \geq T_c^*$), the solid-vapor separation d starts to drop gradually as the temperature increases in Fig. 4(b). When the temperature increases from $T^* = 2.2$ to $T^* = 3.6$, the solid-vapor interface shifts towards the wall surface with a distance of 12.8σ.

C. Thermal-induced Depletion Instability of the Lubricant

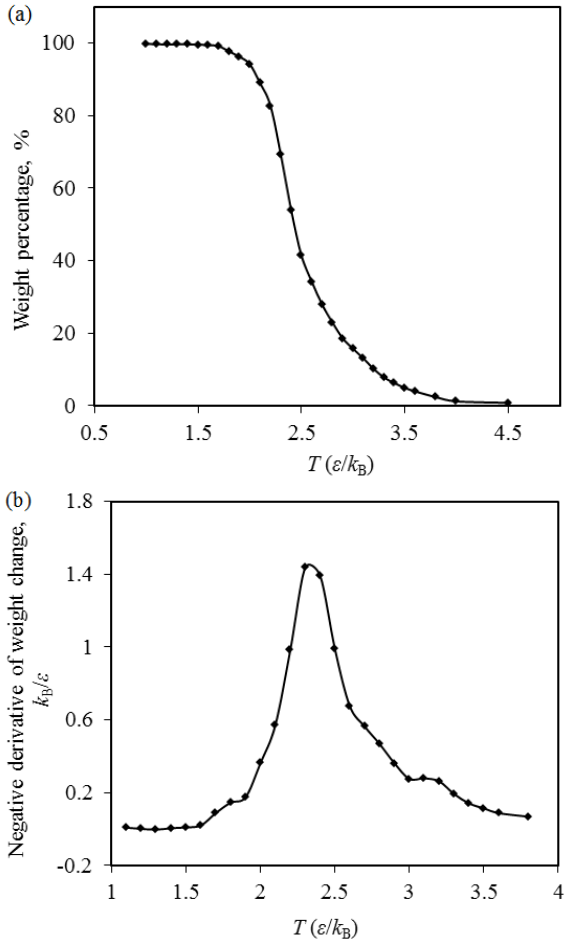

Fig. 5 (a) Weight change of the lubricant as a function of temperature; (b) negative derivative of the lubricant weight change at various temperatures

In our study, we define the thermal stability of the lubricant as the temperature T_{des}^*, at which 5% weight loss is observed. Fig. 5(a) indicates that the thermal stability of nonfunctional lubricant desorption T_{des}^* is about 2.0. Below T_{des}^*, the lubricant is expected to be thermally stable. Otherwise, the lubricant starts to lose its stability and evaporate far away from the HDI. When the temperature increases from $T^* = 2.0$ to $T^* = 3.0$, the

weight loss grows from 5% up to 95%, with an average rate of $0.6k_B/\varepsilon$. Since the lubricant film is modeled by identical beads in all chains and the bonds are assumed to break once the distance is beyond the critical bond length r_b, we should observe a chemical change in the lubricant decomposition. This chemical change corresponds to the step in the weight loss graph in Fig. 5(a). Ji and her coworkers [19] studied the thermal stability of the commercial lubricants Zdol, A20H, and one of their in-house designed and synthesized lubricant, lube 1+. In their work, the thermogravimetric analysis (TGA) curve of lube 1+ is similar to our result, with one weight loss step; while, there are two steps in the TGA curves for lubricants Zdol and A20H, which indicates a more complex chemical change. Figure 5(b) shows the lubricant weight loss rate as a function of temperature. The maximum peak in Fig. 5(b) reveals that the lubricant reaches its largest weight loss rate at $T^* = 2.4$. There may be two reasons to account for the existence of this maximum value. Firstly, about half of the lubricant is observed to evaporate at $T^* = 2.4$based on Fig. 5(a), leaving few lubricant molecules capable of flying away from the wall surface easily. Therefore, when the temperature continues to increase, the attractive wall interaction becomes dominant and adsorbs the remaining lubricant that weakens the evaporation rate. In view of this, once the weight loss rate has reached its maximum value at $T^*= 2.4$, it starts to decrease as the temperature increases. Secondly, at around this peak, lubricant decomposition may occur apart from just evaporation. The lubricant is assumed to have the largest decomposition rate at around $T^* = 2.4$, which constitutes to a decreasing trend of the weight loss rate at $T^*> 2.4$. However, the thermal decomposition profile as shown in Fig. 6 demonstrates that the lubricant begins to decompose at $T^*= 2.6$and reaches its maximum decomposition rate at around $T^* = 3.5$. Therefore, the maximum peak in Fig. 5(b) is attributed to the attractive wall interaction, but not the lubricant decomposition. Furthermore, when $T^*< 2.6$, the weight loss up to 60% is due to the evaporation and elimination of lubricant molecules away from the wall surface. However, in contrast, lubricant decomposition occurs at $T^*> 2.5$, which leads to further weight loss in addition to evaporation.

As seen in Fig. 6, we calculate the temperature at 5% bond loss to investigate the thermal stability of lubricant decomposition. This temperature is denoted as T_{dec}^* and is observed to be $T_{dec}^*= 3.0$. By comparing $T_{dec}^*$with T_{des}^* ($T_{dec}^*= 2.0$), we believe that lubricant desorption is favored over decomposition in our work. When the temperature increases from $T^* = 3.0$ to $T^* = 4.5$, the bondbreakage increases from 5% to 96%. Moreover, at $T^* = 3.0$ (T_{dec}^*), about 84% lubricant molecules evaporate far away from the wall surface (Fig. 5(a)).Under such a condition, the lubricant is probably considered to lose its functionality and ability to protect the wall surface from wear and corrosion damages. Therefore, lubricant desorption is the main cause of the lubricant failure at HDI in our simulations.

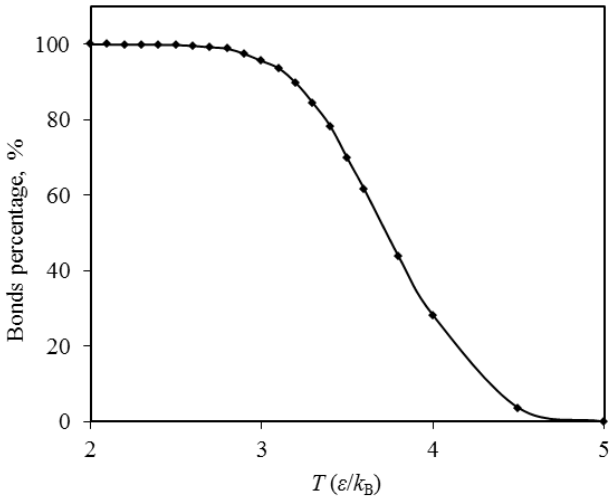

Fig. 6 Decomposition profile of the lubricant

IV. Summary

In this study, the phenomena of the thermal-induced desorption and decomposition of lubricant films have been studied via MD simulation method. To depict lubricant decomposition accurately, a quartic bond potential was employed into a coarse-grained bead-spring polymer model. Based on this novel technique, we evaluated the surface tension density and the number density profiles to verify the lubricant weight loss during heat treatment. The density profile was partially described by a hyperbolic tangent function, which indicates the liquid-vapor interfacial thickness δ. It is observed that both the interfacial thickness δ and solid-vapor separation d increase monotonously with the temperature. However at high temperature, i.e., $T^*> 2.1$, the liquid phase would vanish and we estimated the solid-vapor separation d as the distance, beyond which the density profile starts to approach to the constant vapor density ρ_v. As such, the separation d is found to drop gradually as the temperature increases. Additionally, the lubricant weight and bond loss profiles were examined to study the thermal stability and durability of the lubricant film. It shows that the lubricant desorption is favored over decomposition and is the main cause of the lubricant failure at the HDI.

Acknowledgment

The work described in this paper is supported by a grant from Ministry of Education, Singapore (Project No. RG 13/09).

References

[1] J. Zhou., Y. S. Ma, B. Liu, Q. F. Leng, M. Matsumoto and J. G. Xu, "Flying height-attitude observation and investigation of sliders in load/unload process,"*IEEE Transactions on Magnetics*, vol. 38, pp. 2123-2125, 2002.

[2] S. H. Charap, P. L. Lu and Y. J. He, "Thermal stability of recorded information at high densities,"*IEEE Transactions on Magnetics*, vol. 33, pp. 978-983, 1997.

[3] M. H. Kryder, E. C. Gage, T. W. McDaniel, W. A. Challener, R. E. Rottmayer, G. P. Ju, Y. T. Hsia and M. F. Erden, "Heat assisted magnetic recording,"*Proceedings of the Ieee*,vol. 96, pp. 1810-1835, 2008.

[4] W. A. Challener, C. B. Peng, A. V. Itagi, D. Karns, W. Peng, Y. G. Peng, X. M. Yang, X. B. Zhu, N. J. Gokemeijer, Y. T. Hsia, G. Ju, R. E. Rottmayer, M. A. Seigler and E. C. Gage, "Heat-assisted magnetic recording by a near-field transducer with efficient optical energy transfer,"*Nature Photonics*, vol. 3, pp. 220-224, 2009.

[5] L. Wu, "Modelling and simulation of the lubricant depletion process induced by laser heating in heat-assisted magnetic recording system," *Nanotechnology,* vol. 18, pp. 215702, 2007.

[6] N. Tagawa, R. Kakitani, H. Tani, N. Iketani and I. Nakano, "Study of lubricant depletion induced by laser heating in thermally assisted magnetic recording systems-effect of lubricant film materials," *IEEE Transactions on Magnetics,* vol. 45, pp. 877-882, 2009.

[7] N. Tagawa, H. Andoh and H. Tani, "Study on lubricant depletion induced by laser heating in thermally assisted magnetic recording systems: effect of lubricant thickness and bonding Ratio," *Tribology Letters,* vol. 37, pp. 411-418, 2010.

[8] Y. Li, C. H. Wong, B. Li, S. Yu, W. Hua and W. Zhou, "Lubricant evolution and depletion under laser heating: a molecular dynamics study," *Soft Matter,* vol. 8, pp. 5649-5657, 2012.

[9] P. S. Chung, H. G. Chen and M. S. Jhon, "Molecular dynamics simulation of binary mixture lubricant films," *Journal of Applied Physics,* vol. 103, pp. 07F526-3, 2008.

[10] C. H. Wong, B. Li, S. K. Yu, W. Huaand W. D. Zhou, "Molecular dynamics simulation of lubricant redistribution and transfer at near-contact head-disk interface," *Tribology Letters,* vol. 43, pp. 89-99, 2011.

[11] M. J. Stevens, "Interfacial fracture between highly cross-linked polymer networks and a solid surface: effect of interfacial bond density," *Macromolecules,* vol. 34, pp. 2710-2718, 2001.

[12] M. Tsige and M. J. Stevens, "Effect of cross-linker functionality on the adhesion of highly cross-linked polymer networks: amolecular dynamics study of epoxies," *Macromolecules,* vol. 37, pp. 630-637, 2004.

[13] K. Kremer and G. S. Grest, "Dynamics of entangled linear polymer melts: a molecular-dynamics simulation," *The Journal of Chemical Physics,* vol. 92, pp. 5057-5086, 1990.

[14] J. G. Kirkwood and F. P. Buff, "Thestatisticalmechanicaltheoryof surface tension," *Journal of Chemical Physics,* vol. 17, pp. 338-343, 1949.

[15] D. Stansfield, "The surface tensions of liquid argon and nitrogen," *Proceedings of the Physical Society,* vol. 72, pp. 854-866, 1958.

[16] J. W. Cahn and J. E. Hilliard, "Free energy of a nonuniform system. I. interfacial free energy," *The Journal of Chemical Physics,* vol. 28, pp. 258-267, 1958.

[17] F. P. Buff, R. A. Lovett and F. H. J. Stillinger, "Interfacial density profile for fluids in the critical region," *Physical Review Letters,* vol. 15, pp. 621-623, 1965.

[18] P. Orea, Y. Duda, V. C. Weiss, W. Schroer and J. Alejandre, "Liquid-vapor interface of square-well fluids of variable interaction range," *Journal of Chemical Physics,* vol. 120, pp. 11754-11764, 2004.

[19] R. Ji, T. K. L. Dao, B. X. Xu, J. W. Xu, B. L. Goh, E. Tan, H. Q. Xie and T. Liew, "Lubricant pickup under laser irradiation," *IEEE Transactions on Magnetics,* vol. 47, pp. 1988-1991, 2011.